[Frontiers In Bioscience, Landmark, 22, 1713-1723, June 1, 2017]

FDG PET/CT as theranostic imaging in diagnosis of non-small cell lung cancer

Margarita Kirienko[1], Francesca Gallivanone[2], Martina Sollini[1], Giulia Veronesi[3], Emanuele Voulaz[3], Lidjia Antunovic[4], Lorenzo Leonardi[4], Giorgio Testanera[4], Isabella Castiglioni[2], Arturo Chiti[1, 4]

[1]Department of Biomedical Sciences, Humanitas University, Rozzano, Milan, Italy, [2]IBFM-CNR, Segrate, Milan, Italy, [3]Thoracic Surgery, Humanitas Clinical and Research Center, Rozzano, Milan, Italy, [4]Nuclear Medicine, Humanitas Clinical and Research Center, Rozzano, Milan, Italy

TABLE OF CONTENTS

1. ABSTRACT

Objective of this work was to evaluate the role of 18F-fluorodeoxyglucose (FDG) positron-emission tomography features as theranostic imaging biomarkers in non-small cell lung cancer. In a retrospective protocol, 31 stage I-III NSCLC patients were enrolled. Patients underwent FDG PET/CT for staging purposes before surgery and were followed for two years after surgery. PET images were quantitatively analyzed. For the primary lesion, metabolic tumour volume, maximum standardized uptake value (SUV), SUV corrected for partial volume effect, total lesion glycolysis, 14 histogram and four shape-and-size features were extracted as PET imaging features. PET features were correlated with histology and 2-year disease-free survival (DFS). Significant correlations were found between grading, T parameter, N status, pathological stage and different FDG PET features. Histogram-based features “energy” and “kurtosis” resulted to be predictive for DFS. The cut-off value identified for “kurtosis” was able to separate the adenocarcinoma patients with different outcomes. FDG PET features are able to characterize lung cancer lesions, suggesting the possibility of reliable “imaging biopsy”, and have a predictive role in adenocarcinoma patients undergoing surgery.

2. INTRODUCTION

In recent years, the concept of ‘personalized medicine’ or ‘precision medicine’ emerged. ‘Personalized medicine’ aims to tailor medical interventions, from prevention through diagnosis and treatment, to post-treatment follow-up, at individual level, i.e. on single patient basis, accounting for individual differences in disease susceptibility, as well as in prognosis and response to a specific treatment. As recognized by the European Society of Radiology, medical imaging has a key role toward ‘personalized medicine’, impacting in different ways on this new paradigm of individualized patient care (1).

Medical imaging has greatly evolved from its beginnings. Traditional anatomical medical imaging, allowing to detect morphological and spatial characteristics of the disease, can be now complemented by a wide variety of functional medical imaging techniques, such as Positron Emission Tomography (PET), allowing to evaluate disease biological processes at a molecular level. Technological advancements enable medical imaging devices to detect diseases with high spatial resolution and high signal-to-noise ratio. Furthermore the development of accurate and advanced image

processing methods, both at reconstruction and at a post-reconstruction level, opened to the possibility to perform both qualitative and quantitative assessment of the disease. The ability to process medical images data to extract quantitative data stimulated studies devoted to evaluate of the role of quantitative parameters objectively measured on an image, as surrogate disease biomarkers, the so called 'imaging biomarkers' (2–3). Since the concept of 'personalized medicine' relies both on the personalization of both diagnostic and therapeutical work up, different studies aimed at evaluating imaging biomarkers with a theranostic role, i.e. which have an impact on disease diagnosis, prognosis, monitoring and prediction of treatment response (e.g. 4).

In recent years, advancement in sophisticated image processing methods allowed to apply methods enabling to extract image biomarkers, hidden at human naked eye, which describe image texture and intra-voxel relationships. These complex methodologies, allowing evaluating a large amount of tumor imaging features, are expected to describe tumor phenotype and to be closely related to biological tumor characteristic and to patient outcome. This approach of converting imaging data into a large number of mineable and significant data, containing information on disease pathophysiology is known as radiomics (5).

Evidence has shown that the radiomics approach, through advanced image processing of both computed tomography (CT) and positron emission tomography (PET), is able to provide additional information on tumour phenotype, therapeutic response and prognosis in head and neck, oesophageal, breast, pancreas, and non-small cell lung cancer (NSCLC) patients in different clinical settings (6–12). Ha *et al.* identified 15 FDG PET textural features displaying significantly different values between adenocarcinoma (n=17) and squamous cell carcinoma (n=13). Linear discriminant analysis with 24 features accurately separated the two subtypes (13). Specific FDG textures were associated with non-response to therapy and worse prognosis in 53 NSCLC patients treated with chemo-radiotherapy (14). The ability of textural features to predict treatment response to erlotinib was evaluated in 47 patients at baseline and 6 weeks after start of treatment. A reduced "heterogeneity" was found to be associated with response, and changes in first-order "entropy" with overall survival (OS) and response (15). Tixier *et al.* found that textural features were associated with poorer OS and recurrence-free survival in 102 patients treated with surgery, chemotherapy and/or radiation therapy (RT) (16). Fried *et al.* found FDG PET/CT features to be associated with OS in stage III disease patients undergoing RT. Moreover, OS predictors generated using both imaging features and conventional prognostic factors permitted improved risk stratification (17). Pyka *et al.* found "entropy" to be predictive for disease-specific survival in 45 patients with early-stage disease who were undergoing stereotactic RT (18). In another work "dissimilarity" was found to be a strong predictor of disease-specific survival and disease-free survival (DFS) in patients undergoing RT (19). Desseroit *et al.* exploited tumour heterogeneity on CT and PET images in order to develop a nomogram to predict patient outcome. In this retrospective study including 116 patients treated with surgery, chemotherapy and/or RT, the authors found that addition of PET "entropy" and CT "zone percentage" into the nomogram improved patient stratification amongst those with stage II and III disease, enabling identification of patients with the poorest prognosis (20).

Despite the aforementioned results, data on the correlations between FDG PET features and pathology, staging and clinical outcome in treatment-naïve NSCLC patients are lacking. The aim of the present study was to evaluate the ability of FDG PET features derived from texture analysis to characterize NSCLC lesions assessing the correlations with histological data, and to predict outcome in early-stage patients undergoing primary surgery.

3. MATERIALS AND METHODS

3.1. Patients

We retrospectively analyzed patients' clinical and imaging data, extracted from the institutional database, from April 2012 until January 2013. Inclusion criteria were: (a) histological diagnosis of NSCLC, (b) primary surgical intervention with curative intent and (c) staging FDG PET/CT performed within 1 month before surgery. Exclusion criteria were: (a) other cancer diagnosis during the previous 3 years, (b) distant metastases at diagnosis, (c) no follow-up data available and (d) death unrelated directly to lung cancer progression. We identified 31 patients (M:F=25:6, mean age 68±9 years). The institutional ethics committee approved the study.

The patients' lesion characteristics are summarized in table 1.

3.2. FDG PET/CT imaging protocol

FDG PET/CT image acquisition was performed 60±5 min after FDG administration, according to the European Association of Nuclear Medicine (EANM) guidelines (21).

Images were acquired on a General Electric Discovery PET/CT 690 equipped with LYSO crystals and a 64-slice CT (General Electric Healthcare, Waukesha, WI, USA), accredited within the EARL programme (www.eanm.org). CT images without

Table 1. Lesion characteristics

Pathology		Frequency	%
Type	Adenocarcinoma	19	61%
	Squamous cell carcinoma	9	29%
	Other[1]	3	10%
Grading	G1	1	3%
	G2	13	42%
	G3	16	52%
	Not available	1	3%
Primary lesion (T)	T1	10	32%
	T2	16	51%
	T3	4	13%
	T4	1	3%
Lymph node status (N)	N0	19	61%
	Other	12	39%
Stage	IA	7	23%
	IB	7	23%
	IIA	6	19%
	IIB	3	10%
	IIIA	8	26%

n=31 patients, [1]: colloid adenocarcinoma (n=1), adenosquamous carcinoma (n=1) and unspecified NSCLC (n=1)

contrast enhancement or respiratory gating (free-breathing images) were acquired. The CT attenuation correction acquisition parameters were 140 kV voltage, 140 mA tube current and 3.7.5 mm slice thickness. PET data were acquired using 2 min/bed position with a 256×256 matrix and a voxel size of 2.7.3×2.7.3×3.2.7 mm3. Images were reconstructed using Vue Point Fx (VPFX, fully 3D time-of-flight iterative reconstruction) with Sharp IR Algorithm implemented. All PET images were corrected for attenuation using the acquired CT data.

3.3. FDG PET/CT analysis

Qualitative analysis of FDG PET images was performed by two experienced board-certified nuclear medicine physicians (MS and MK, 10-years and 8-years' experience in reading PET/CT scans), in order to identify spatial extension of primary tumour. Quantification of FDG PET parameters was performed using a home-made image processing tool, running on Matlab (22).

Metabolic tumour volume (MTV) was delineated using a fully automatic image segmentation method, combining an automatic threshold-based algorithm for the definition of MTV and a k-means clustering algorithm for estimation of the background. The method was previously calibrated and validated on a variety of PET/CT scanners, including the GE Discovery PET/CT 690, and on a variety of lesions, spherical or non-spherical with homogeneous or non-homogeneous FDG uptake, showing an accuracy of up to 92% (23). MTV was obtained as the number of PET voxels multiplied by the volume of the voxel in the PET image (cc). Average and maximum standardized uptake value (SUV_{max}) of the primary lesion were calculated within the segmented MTV. Mean SUV was corrected for partial volume effect (PVC-SUV_{mean}) (24) and total lesion glycolysis (TLG) was calculated as the product between PVC-SUV_{mean} and MTV, resulting in a TLG value corrected for the partial volume effect.

Fourteen features were extracted as first-order statistics features, describing the characteristics of the histogram of the PET voxel intensities: energy, entropy, kurtosis, maximum, mean, mean absolute deviation, median, minimum, range, root mean square, skewness, standard deviation, uniformity and variance (8). Four features describing the shape and size of the segmented MTV were extracted: surface area, spherical disproportion, sphericity and surface-to-volume ratio (8).

3.4. Follow-up

Survival time was estimated starting from date of surgery and 2-year DFS was calculated.

Table 2. FDG PET features

Feature	Range	Mean	SD[1]
SUV_{mean} (g/cc)	2.7.–22.0.	11.2.	4.8.
SUV_{max} (g/cc)	2.3.–27.6.	13.8.	6.7.
MTV (cc)	1.5.–137.6.	29.2.	31.2.
TLG (g)	4.1.–1223.4.	340.7.	368.3.
Energy $((g/cc)^2)$	2.2.E03–7.8.E06	1.3.E06	1.9.E06
Entropy	6.7.–7.5.	7.5.	0.3.
Kurtosis	2.0.–7.3.	3.0.	1.1.
Maximum (g/cc)	2.3.–27.6.	13.8.	7.0.
Mean (g/cc)	1.4.–15.2.	6.1.	3.3.
Mean absolute deviation (g/cc)	0.2.–4.9.	2.3.	1.3.
Median (g/cc)	1.3.–15.4.	5.8.	3.3.
Minimum (g/cc)	0.7.–3.3.	1.5.	0.6.
Range (g/cc)	1.1.–25.0.	12.8.	6.6.
RMS (g/cc)	1.4.–15.9.	6.7.	3.5.
Skewness	-0.8.–2.0.	0.6.	0.5.
Standard deviation (g/cc)	0.2.1–5.7.	2.7.	1.5.
Uniformity	4.6.E-03–1.2.E-02	6.5.E-03	1.8.E-03
Variance $((g/cc)^2)$	0.0.4–33.0.	9.7.	8.7.
Surface area (cm^2)	11.7.–472.0.	8.9.E+01	9.1.E+01
Spherical disproportion	1.5.–3.7.	1.9.	0.4.
Sphericity	0.3.–0.7.	5.4.E-01	9.3.E-02
Surface to volume ratio (cm^{-1})	2.1.–7.7.	3.7.	1,1

[1]: standard deviation

At 2 years from the surgical procedure, 19 of the 31 patients (61%) had no evidence of disease, nine (29%) showed relapse (distant site relapse in five cases and local disease relapse in four), two (6%) had died and one (3%) had been lost to follow-up (last follow-up data 20 months after surgery, without evidence of disease). At the last follow-up (29±10 months) 16 of the 31 patients (52%) had no evidence of disease while 13 (42%) had disease recurrence (concomitant local and distant recurrence in one case, distant or local site relapse in six cases each) and two (6%) had died.

3.5. Statistical analysis

Univariate analysis was used to determine the relationship between FDG PET features and histology (type and grading) as well as AJCC stage. Univariate analysis was performed to assess the relationship between each PET parameter and 2-year DFS. A multivariate approach was not tested owing to the number of PET parameters evaluated (n=22) and the number of patients considered (n=31). One-to-one ROC analysis was used to look for possible cut-off values for each PET parameter against each outcome endpoint. Subsequently, Kaplan-Meier analysis and log rank test were used to test the ability of the identified cut-off values to stratify patients with different outcomes. A p-value < 0.0.5 was considered significant.

4. RESULTS

4.1. Patients

All lung lesions showed FDG uptake at qualitative analysis of PET images. Image analysis was performed in all patients. Average and range of PET features are summarized in table 2.

4.2. FDG PET features and histology

Histology, lymph node status (N) and AJCC stage were mainly related to first-order statistics metrics while grading and extent of the tumour (T) were primarily related to geometrical features. Compared with other parameters, lymph node status (N) was correlated with a higher number of features. Table 3 shows statistically significant correlations, identified in the univariate analysis, between FDG PET features and histology and stage. Figure 1 shows a case of a patient with a visually heterogeneous lung lesion.

Table 3. Significant correlations resulted from the univariate analysis among FDG PET features and histological data

Pathology	PET feature	Significance (*p*)
AdC[1] vs SqCC[2]	Mean absolute deviation	<0.0.5
Grading (G1 vs G2 vs G3)	$PVC\text{-}SUV_{mean}$	0.0.5
	Spherical disproportion	0.0.1
	Sphericity	0.0.1
Primary tumour (T) T1 vs other	MTV	<0.0.5
	Surface	<0.0.5
	Surface-to-volume ratio	<<0.0.5
Lymph nodes (N) N0 vs other	$PVC\text{-}SUV_{mean}$	<0.0.5
	SUV_{max}	0.0.1
	PVC-TLG	<0.0.1
	Maximum	<0.0.5
	Mean	<0.0.5
	Minimum	<0.0.5
	Energy	0.0.05
	Kurtosis	<0.0.5
	Standard deviation	0.0.1
	Variance	0.0.1
Stage (I vs II vs III)	Mean absolute deviation	<0.0.5
	Energy	0.0.05

[1]: AdC, adenocarcinoma; [2]: SqCC, squamous cell carcinoma

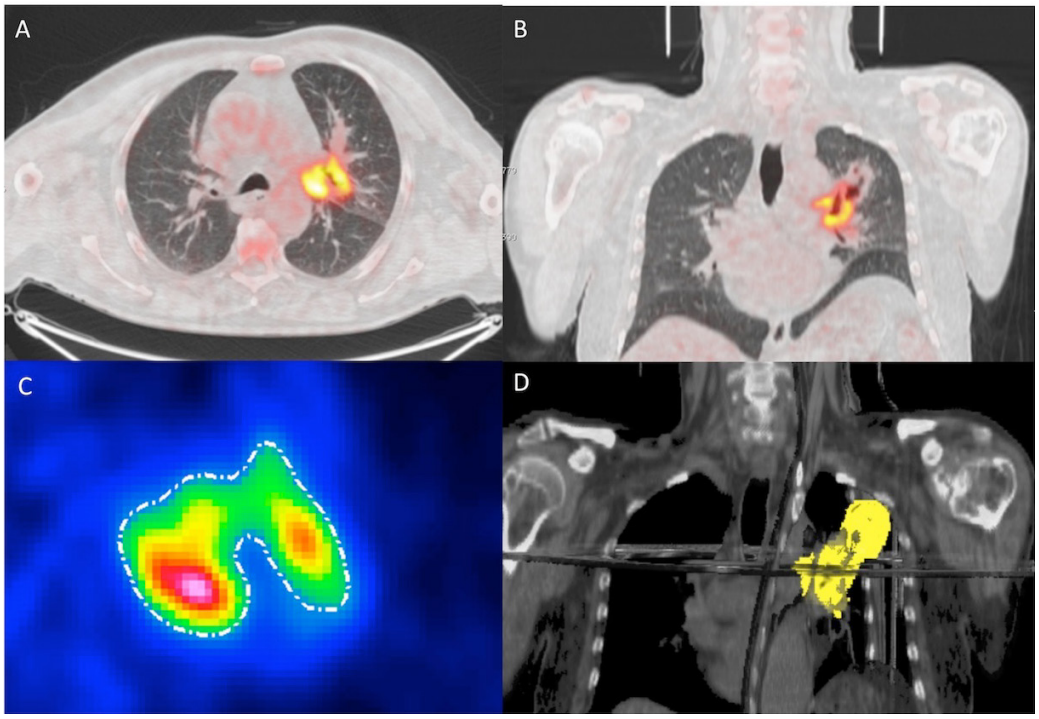

Figure 1. A 67-year-old male with squamous cell carcinoma, G3pT3N1 (stage IIIa) who underwent pneumonectomy and subsequent adjuvant chemotherapy with cisplatin and vinorelbine. After 36 months' follow-up the patient had no evidence of disease. PVC-SUV = 15.59 g/cc, SUVmax = 21.18 g/cc, Energy = 3.2E06 (g/cc)2, Entropy = 4.08, Kurtosis = 3.85. The axial (A) and coronal (B) fused PET/CT images show the lesion in the upper left lobe; the axial PET (C) image shows the tumour segmentation operated by the algorithm; (D) metabolic tumour volume visualized on CT images.

Table 4. Statistically significant correlations between FDG PET parameters and DFS identified by the ROC

Survival endpoint	PET feature	P value	Cut-off	Sensitivity	Specificity
Disease-free survival	Energy ((g/cc)2)	<0.0.5	3.2.2E05	71%	73%
	Kurtosis	<0.0.5	2.7.44	86%	64%

4.3. FDG PET features and survival

Survival analysis was performed considering 2-year DFS. Two-year DFS allowed comparison of follow-up data in the majority of patients (28/31). One patient was considered lost to follow-up (last data available 20 months after surgery), and a further two patients were excluded from the survival analysis because they had been diagnosed with a second NSCLC in the contralateral lung 2 months after the first surgery. Histopathological characteristics of the first and the second lesion differed in both patients; thus the contralateral lesion was considered a different tumour rather than a metastases from the first NSCLC. Although both patients were treated with surgery with curative intent twice, they were excluded from the survival analysis due to the impossibility of identifying which tumour was responsible for the outcome (no evidence of disease and relapse 25 and 21 months after the first surgery, respectively).

PET features were found not to be related to 2-year DFS in the 28 patients analyzed. Based on the significant correlation found between the PET feature "mean absolute deviation" and histology (p<0.0.5), a second analysis was performed limiting the test to the adenocarcinoma patients, who represented the largest group (19/31). Also for this analysis we excluded the patients with two metachronous NSCLCs; thus 17/31 patients were analysed. In this subgroup of adenocarcinoma patients, mean duration of follow-up was 30±8 months. At 2 years from the surgical procedure, 12 of the 17 patients (71%) had no evidence of disease while five (29%) showed relapse (three at local and two at distant sites). At the last follow-up, ten of these 17 patients (59%) had no evidence of disease, six (35%) had experienced disease recurrence and one (6%) had died.

Statistically significant correlations between FDG PET features and DFS identified by the ROC analysis are reported in table 4.

Both "energy" and "kurtosis" were found to be predictive for DFS. Cut-off values for these parameters, able to separate the whole population into two groups with different outcomes, were identified. Using the log rank test, only "kurtosis" was able to stratify patients with significantly different DFS. The DFS curve of patients with a primary lesion showing histogram kurtosis <2.7.44 was significantly different from that of patients with histogram kurtosis ≥2.7.44 (p<0.0.5). The DFS curve of patients with a primary lesion showing histogram energy <$3.2.2\times10^5$ $(g/cc)^2$ was not significantly different from that of patients with a histogram energy ≥ $3.2.2\times10^5$ (p>0.0.5).

5. DISCUSSION

Advanced features of medical imaging are emerging as effective quantitative indexes able to assist diagnosis, treatment response and survival analysis in NSCLC. The present study, through the assessment of the correlations between FDG PET features and histology, staging and clinical outcome in NSCLC patients undergoing surgery with curative intent, shows that FDG PET texture analysis is feasible, is able to characterise *in vivo* NSCLC lesions and can predict outcome in adenocarcinoma patients. These findings are in line with those of previous studies that compared PET parameters obtained by static versus parametric acquisitions (25) and that evaluated correlations between PET features and disease stage (26) and between PET features and patient outcome (27).

In contrast to the study by Ha *et al.* (13) in our series of patients only one feature was found to be significantly associated with histological type. This is probably attributable to the disproportionate number of adenocarcinomas in the sample (19) as compared with squamous cell carcinomas (nine), which may have translated into an underestimation of significance.

On the other hand, histological grade was found to be significantly correlated with the geometrical PET features "sphericity" and "spherical disproportion", suggesting that poorly differentiated lesions have an asymmetrical shape corresponding to a more asymmetrical growth.

Considering the pathological AJCC stage, the T parameter correlated with MTV and the geometrical feature "surface-to-volume ratio", demonstrating that imaging is consistent with the real tumour dimensions and shape. However, the T1 lesions were compared with a group that combined T2, T3 and T4 lesions. This choice was based on statistical considerations, in that comparison of small groups with different sample sizes was considered unreliable. Nevertheless, our preliminary results are encouraging and provide the rationale for further analysis testing the differentiation among different T groups in a larger patient cohort.

Accurate preoperative staging of mediastinal lymph nodes in patients with potentially resectable NSCLC is of paramount importance. FDG PET/CT is crucial in this setting, as it is more accurate (overall sensitivity, 78%–93%; specificity, 82%–95%) than CT (sensitivity, 55%–57%; specificity, 81%–82%) (28–30). According to the American College of Chest Physicians Evidence-Based Clinical Practice Guidelines,(24) if FDG PET/CT in the mediastinum is negative, invasive sampling may even be omitted in selected patients, since FDG PET/CT shows a false negative rate of only approximately 5% (range 3%–6%) (31–34). This especially holds true in the case of peripheral tumours (outer third of the lung) ≤3 cm.(26–28) For tumours >3 cm (mainly adenocarcinomas), further mediastinal staging techniques providing histology should be considered even without enlarged (hilar and/or mediastinal) lymph nodes on CT imaging and with PET-negative nodes (34). In our study many PET features were found to be related to the presence of lymph node metastases. These findings assume a high clinical relevance. In fact, the possibility of predicting lymph node status through characterisation of the primary lung lesion on the basis of PET textural features may obviate the need for further mediastinal staging techniques. The textural feature "kurtosis" is of particular interest since it is a measure of histogram sharpness within the lesion; thus, it is indirectly a measure of uptake uniformity within the lesion at the voxel level. These results could further support clinicians in treatment decision-making.

Additionally, we found a correlation between the textural features "mean absolute deviation" and "energy" and pathological AJCC stage (stage I versus II versus III). Stage is one of the main prognostic factors in NSCLC and guides treatment strategy (35). Our results are in line with those in the recent study by Desseroit *et al.* in which a nomogram, incorporating clinical stage III, large tumour volume and textural features extracted from both PET and CT, had a higher stratification power than staging alone and was able to stratify patients with stage II and III disease, thereby identifying patients with the poorest prognosis (20).

Overall, these results may be of high relevance in clinical practice. The TNM stage is defined according to the TNM staging system after tumour resection, whereas in a larger number of NSCLC patients, who receive as primary treatment neo-adjuvant chemotherapy and/or radiotherapy, just clinical staging is possible. A strong correlation between PET features, histology, grading and staging (with specific regard to the N status), if confirmed in a larger series of patients, may really change the scenario of NSCLC management in that reliable *in vivo* "imaging biopsy" by routine baseline FDG PET/CT may be feasible.

Recent papers have reported that quantification of tumour heterogeneity may provide information that could improve prediction of response to therapy and prognostic evaluation in patients with NSCLC (14, 16–19, 27, 36–41). In our series, PET features ("energy" and "kurtosis") proved capable of predicting patient outcome in adenocarcinoma patients. Both these image parameters should be considered as parameters reflecting the shape of histogram distribution allowing to identify histogram dominated by a single value and histograms with predominantly random distribution, thus giving information on signal heretogeneity. Similarly, Kim *et al.*(41), evaluating the prognostic significance of intratumoral metabolic heterogeneity on pretreatment FDG PET/CT in pathologically N0 NSCLC patients after curative surgical resection, found that both standard metabolic parameters (i.e. SUV_{max}, MTV, TLG) and intratumoral heterogeneity can predict recurrence in patients with adenocarcinomas but not in those with squamous cell carcinomas. Additionally, in the present study the cut-off identified for "kurtosis" was able to stratify patients with different DFS with high sensitivity, even if with limited specificity. More interestingly, one of the most widely used PET parameters, SUV_{max}, was found not to be related to DFS, and this was also true for PVC-SUV. Similarly, Apostolova *et al.* found "asphericity" to be a strong independent predictor of outcome while none of the conventional PET metabolic parameters (SUV_{max}, SUV_{mean}, MTV and TLG) showed a significant predictive value (27). These findings support the idea that textural features could be more accurate in prognostication of patient outcome.

The presence of partial volume effect on the PET images is a physical limitation that strongly affects uptake estimation within structures up to 8–15 mm in diameter (42). Any method to characterise heterogeneity will treat partial volume effect and therefore PVC should be applied prior to calculating the histogram (43). However, PVC is not routinely applied either in the clinical setting or in texture analysis studies. To overcome the potential impact of partial volume effect, some authors have evaluated only lung lesions with a metabolically active tumour volume >3 cm^3 or at least 30 mm in maximum diameter (16, 25, 44). In the present study, a fully automatic PVC method was applied for both SUV_{mean} and TLG (24). Moreover, in order to accurately and consistently define the lesion volume, we used a fully automatic image segmentation method validated using 3D printed anthropomorphic phantoms (including non-spherical and non-uniform objects). The majority of PET segmentation strategies have been validated in ideal conditions (e.g. in spherical objects with uniform radioactivity distribution), while the majority of cancer lesions do not have these characteristics. Therefore, the use of anthropomorphic phantoms allowed us to mime realistic conditions. Additionally, this segmentation

method has been calibrated and validated on a variety of PET/CT scanners, including the GE Discovery PET/CT 690 (23). The combination of these strategies guaranteed accurate and reproducible quantitation of PET features, including among different operators.

The accurate quantification of texture features may be hindered by respiratory motion in lung cancer patients. Motion induce image blurring in static PET images (3D PET) leading to reduction in tumor uptake and overestimation of metabolic tumor volume. Respiratory-gated (4D PET) imaging gates PET image acquisition with respiratory motion in order to improve PET image quality and has been shown to reduce motion blurring in the PET images, providing more accurate quantification of lung tumor activity. Texture features are likely to be blurred during 3D PET acquisition of lung tumors. Yip S *et al.* (2014) (45) found significant differences in "maximal correlation coefficient", "long run low gray-level emphasis", "coarseness", and "busyness" (NGTDM-based) between 3D and 4D PET imaging. When measuring tumor heterogeneity characteristics, reduced motion blurring by 4D PET acquisition was found to offer significantly better spatial resolution of textural features. Different results have been reported by Cheng NM *et al.* (2016) (46), who compared the attenuation correction of PET images with helical CT (PET/HCT) and respiration-averaged CT (PET/ACT) in 56 NSCLC patients. PET/ACT yielded significantly higher SUV_{max}, SUV_{mean}, and TLG while significant differences between PET/HCT and PET/ACT were not observed with regard to other features, including "$entropy_{Hist}$", "$entropy_{GLCM}$", "dissimilarity", "$homogeneity_{GLCM}$", and "uniformity" (GLCM-based), "gray-level non-uniformity", "zone-size non-uniformity", and "high gray-level large zone emphasis" (GLSZM-based), and "coarseness", "busyness", "$contrast_{NGTDM}$", and "complexity" (NGTDM-based). A recent work by Grootjans W *et al* (2016) (47) investigated the influence of respiratory motion on quantification of textural parameters reflecting intratumor heterogeneity in patients with lung cancer. The authors performed both gated and non-gated PET scans and they showed that in particular in lower lung lobes, respiratory motion significantly affected quantitative biomarkers. Despite this, considering the overall survival, they found that some heterogeneity descriptors are independent significant covariates in a Cox regression model, in both acquisitions. Carles M *et al.* (2016) (48) evaluated the impact of time-bins in gated (4D-) PET/CT B in heterogeneity quantification, using a synthetic phantom. The authors proposed an optimization of acquisition parameters for accounting lesion motion in thorax district. Despite this, other phantom measurements, with a known gold standard in terms of heterogeneity, should be carried out to evaluate the impact of movement on advanced image-derived parameters.

The term "heterogeneity" conveys different meanings depending on the imaging modality used. In FDG PET, heterogeneity refers to the spatial distribution of radiopharmaceutical uptake, which can at least partly reflect underlying biological processes such as metabolism, hypoxia, angiogenesis, necrosis and cellular proliferation (37–38). "Heterogeneity" is a term frequently used in the reporting of texture analysis results; however, many textural features extracted by different approaches (e.g. histogram-based or gray-level matrix-based) are reported in the literature (49). Although radiomics analysis of medical images shows very promising results, standardization of texture analysis, in terms of methods applied and features extracted, and data reporting is needed in order to validate this tool for multicenter trials.

The present study has limitations: it is retrospective and evaluated a limited number of patients. Nonetheless, our study benefitted from: a homogeneous treatment regimen in the patient cohort, availability of pathological stage and grading from surgical specimens for all patients, fully automatic image segmentation and partial volume effect correction methods and long duration of follow-up.

In conclusion, texture analysis seems capable of characterizing preoperatively lung cancer lesions with respect to histological grading, histological type, stage and lymph node involvement, suggesting the possibility of a reliable *in vivo* "imaging biopsy" by means of routine baseline FDG PET/CT. Moreover, it is predictive of DFS in treatment-naïve adenocarcinoma patients undergoing surgery.

6. ACKNOWLEDGEMENT

Margarita Kirienko and Francesca Gallivanone contributed equally to this paper.

7. REFERENCES

1. European Society of Radiology (ESR) Medical imaging in personalised medicine: a white paper of the research committee of the European Society of Radiology (ESR) *Insights Imaging.* 6(2):141–55 (2015)

2. European Society of Radiology (ESR) ESR Position Paper on Imaging Biobanks. *Insights Imaging.* 6(4):403–10 (2015)

3. JW. Prescott. Quantitative imaging biomarkers: the application of advanced image processing and analysis to clinical and preclinical decision making. *J Digit Imaging.* 26(1):97–108 (2013)

4. W. Ma, J. Jia, S. Wang, W. Bai, J.Yi, M. Bai, Z. Quan, Z. Yin, D. Fan, J. Wang, *et al.*

The Prognostic Value of ^{18}F-FDG PET/CT for Hepatocellular Carcinoma Treated with Transarterial Chemoembolization (TACE) *Theranostics.* 4(7): 736–744 (2014)

5. Gillies RJ, Kinahan PE, Hricak H. Radiomics: Images Are More than Pictures, They Are Data. *Radiology.* 278(2):563–77 (2016)

6. W. Guo, H. Li, Y. Zhu Y, Yang S, Drukker K, Morris E, Burnside E, Whitman G, Giger ML, Ji Y, Tcga Breast Phenotype Research Group. Prediction of clinical phenotypes in invasive breast carcinomas from the integration of radiomics and genomics data. *J Med imaging Bellingham*.2:041007 (2015)

7. A. Cunliffe, SG. Armato, R. Castillo, N. Pham, T. Guerrero, HA Al-Hallaq. Lung texture in serial thoracic computed tomography scans: correlation of radiomics-based features with radiation therapy dose and radiation pneumonitis development. *Int J Radiat Oncol Biol Phys*. 91:1048–56 (2015)

8. HJ. Aerts, ER. Velazquez, RT. Leijenaar, C. Parmar, P. Grossmann, S. Carvalho, J. Bussink, R. Monshouwer, B. Haibe-Kains, D. Rietveld, *et al.* Decoding tumour phenotype by noninvasive imaging using a quantitative radiomics approach. *Nat Commun*. 5:4006 (2014)

9. J. Wang, F. Kato, N. Oyama-Manabe, R. Li, Y. Cui, KK. Tha, H. Yamashita, K. Kudo, H. Shirato. Identifying Triple-Negative Breast Cancer Using Background Parenchymal Enhancement Heterogeneity on Dynamic Contrast-Enhanced MRI: A Pilot Radiomics Study. *PLoS One*. 10:e0143308 (2015)

10. SS. Yip, TP. Coroller, NN. Sanford, H. Mamon, HJ Aerts, RI Berbeco. Relationship between the Temporal Changes in Positron-Emission-Tomography-Imaging-Based Textural Features and Pathologic Response and Survival in Esophageal Cancer Patients. *Front Oncol*. 6:72 (2016)

11. SH. Hyun, HS. Kim, SH. Choi, DW. Choi, JK. Lee, KH. Lee, JO. Park, KH. Lee, BT. Kim, JY. Choi. Intratumoral heterogeneity of (18) F-FDG uptake predicts survival in patients with pancreatic ductal adenocarcinoma. *Eur J Nucl Med Mol Imaging*. 43:1461–8 (2016)

12. K. Rahim, SE. Kim, H. So, HJ. Kim, GJ. Cheon, ES. Lee, KW. Kang, DS. Lee. Recent Trends in PET Image Interpretations Using Volumetric and Texture-based Quantification Methods in Nuclear Oncology. *Nucl Med Mol Imaging*. 48:1–15 (2014)

13. S. Ha, H. Choi, GJ. Cheon, KW. Kang, JK. Chung, EE. Kim, DS. Lee. Autoclustering of Non-small Cell Lung Carcinoma Subtypes on 18F-FDG PET Using Texture Analysis: A Preliminary Result. *Nucl Med Mol Imaging*. 48:278–86 (2014)

14. GJ. Cook, C. Yip, M. Siddique, V. Goh, S. Chicklore, A. Roy, P. Marsden, S. Ahmad, D. Landau. Are Pretreatment 18F-FDG PET Tumor Textural Features in Non–Small Cell Lung Cancer Associated with Response and Survival After Chemoradiotherapy? *J Nucl Med*. 54:19–26 (2013)

15. GJ Cook, ME. O'Brien, M. Siddique, S. Chicklore, HY. Loi, B. Sharma, R. Punwani, P. Bassett, V. Goh, S. Chua. Non-Small Cell Lung Cancer Treated with Erlotinib: Heterogeneity of (18)F-FDG Uptake at PET-Association with Treatment Response and Prognosis. *Radiology.* 276:883–93 (2015)

16. F. Tixier, M. Hatt, C. Valla, V. Fleury, C. Lamour, S. Ezzouhri, P. Ingrand, R. Perdrisot, D. Visvikis, CC. Le Rest. Visual Versus Quantitative Assessment of Intratumor 18F-FDG PET Uptake Heterogeneity: Prognostic Value in Non-Small Cell Lung Cancer. *J Nucl Med*. 55:1235–41 (2014)

17. DV. Fried, O. Mawlawi, L. Zhang, X. Fave, S. Zhou, G. Ibbott, Z. Liao, LE. Court. Stage III Non-Small Cell Lung Cancer: Prognostic Value of FDG PET Quantitative Imaging Features Combined with Clinical Prognostic Factors. *Radiology*.278:214–22 (2016)

18. T. Pyka, RA. Bundschuh, N. Andratschke, B. Mayer, HM. Specht, L Papp, N. Zsótér, M. Essler. Textural features in pre-treatment (F18)-FDG-PET/CT are correlated with risk of local recurrence and disease-specific survival in early stage NSCLC patients receiving primary stereotactic radiation therapy. *Radiat Oncol*. 10:100 (2015)

19. P. Lovinfosse, ZL. Janvary, P. Coucke, S. Jodogne, C. Bernard, M. Hatt, D. Visvikis, N. Jansen, B. Duysinx, R. Hustinx. FDG PET/CT texture analysis for predicting the outcome of lung cancer treated by stereotactic body radiation therapy. *Eur J Nucl Med Mol Imaging*. 43:1453–60 (2016)

20. MC. Desseroit, D. Visvikis, F. Tixier, M. Majdoub, R. Perdrisot, R. Guillevin, C. Cheze Le Rest, M. Hatt. Development of a nomogram combining clinical staging with (18)F-FDG PET/CT image features in non-small-cell lung cancer stage I-III. *Eur J Nucl Med Mol Imaging*. 43:1477–85 (2016)

21. R. Boellaard, R. Delgado-Bolton, WJ. Oyen, F. Giammarile, K. Tatsch, W. Eschner, FJ. Verzijlbergen, SF. Barrington, LC. Pike, WA. Weber *et al.* FDG PET/CT: EANM procedure guidelines for tumour imaging: version 2.0. *Eur J Nucl Med Mol Imaging*. 42:328–54 (2014)

22. A. Stefano, F. Gallivanone, E. Grosso E, C. Messa, L. Gianolli, MC. Gilardi, I. Castilgioni. TOUCH-SUV: a Touchscreen-Assisted Tool for Quantitative, Reproducible, Clinically Feasible and Collaborative Diagnostic Reporting of Whole-Body PET-CT. *Softw Eng*. 1:1–8 (2011)

23. F. Gallivanone, M. Interlenghi, C. Canervari, I. Castiglioni. A fully automatic, threshold-based segmentation method for the estimation of the Metabolic Tumor Volume from PET images: validation on 3D printed anthropomorphic oncological lesions. *J Instrum*. 11:C01022–C01022 (2016)

24. F. Gallivanone, C. Canevari, L. Gianolli, C. Salvatore, PA. Della Rosa, MC. Gilardi, I. Castiglioni I. A partial volume effect correction tailored for 18F-FDG-PET oncological studies. *Biomed Res Int*. 2013:780458 (2013)

25. F. Tixier, D. Vriens, C. Cheze-Le Rest, M. Hatt, JA. Disselhorst, WJ. Oyen, LF. de Geus-Oei, EP. Visser, D. Visvikis. Comparison of tumor uptake heterogeneity characterization between static and parametric 18F-FDG PET images in Non-Small Cell Lung Cancer. *J Nucl Med*. 57:1033–9 (2016)

26. O. van Gómez López, AM. Garcia Vicente, AF Honguero Martínez, AM. Soriano Castrejón, GA. Jiménez Londoño, JM. Udias, P. León Atance. Heterogeneity in (18 F) fluorodeoxyglucose positron emission tomography / computed tomography of non – small cell lung carcinoma and its relationship to metabolic parameters and pathologic staging. *Mol Imaging*. 13:1–12 (2014)

27. I. Apostolova, J. Rogasch, R. Buchert, H. Wertzel, HJ. Achenbach, J. Schreiber, S. Riedel, C. Furth, A. Lougovski, G. Schramm, *et al.* Quantitative assessment of the asphericity of pretherapeutic FDG uptake as an independent predictor of outcome in NSCLC. *BMC Cancer*. 14:896 (2014)

28. EM. Toloza, L. Harpole, DC. McCrory. Noninvasive staging of non-small cell lung cancer: a review of the current evidence. *Chest*. 123(Suppl 1):137S– 146S (2003)

29. GA. Silvestri, MK. Gould, ML. Margolis, LT. Tanoue, D. McCrory, E. Toloza, F. Detterbeck, American College of Chest Physicians. Noninvasive staging of non-small cell lung cancer: ACCP evidenced-based clinical practice guidelines (2nd edition) *Chest.* 132(Suppl 3):178S–201S (2007)

30. GA Silvestri, AV. Gonzalez, MA. Jantz, ML. Margolis, MK. Gould, LT. Tanoue, LJ. Harris, DC. Methods for staging non-small cell lung cancer: Diagnosis and management of lung cancer, 3rd ed: American College of Chest Physicians evidence-based clinical practice guidelines. *Chest.* 143(5 Suppl):e211S – 50S (2013)

31. A. Gómez-Caro, M. Boada, M. Cabañas, M. Sanche, P. Arguis, F. Lomeña, J. Ramirez, L. Molins. False-negative rate after positron emission tomography/computer tomography scan for mediastinal staging in cI stage non-small-cell lung cancer. *Eur J Cardiothorac Surg*. 42:93–100 (2012)

32. PC. Lee, JL. Port, RJ. Korst, Y. Liss, DN. Meherally, NK. Altorki. Risk factors for occult mediastinal metastases in clinical stage I non-small cell lung cancer. *Ann Thorac Surg*. 84:177–81 (2007)

33. J. Wang, K. Welch, L. Wang, FM. Kong. Negative predictive value of positron emission tomography and computed tomography for stage T1–2N0 non-small-cell lung cancer: a meta-analysis. *Clin Lung Cancer*. 13:81–9 (2012)

34. P. De Leyn, C. Dooms, J. Kuzdzal, D. Lardinois, B. Passlick, R. Rami-Porta, A. Turna, P. Van Schil, F. Venuta, D. Waller D *et al.* Preoperative mediastinal lymph node staging for non-small cell lung cancer: 2014 update of the 2007 ESTS guidelines. *Transl lung cancer Res*. 3:225–33 (2014)

35. F. Gester, A. Paulus, AL. Sibille, JL. Corhay, B. Duysinx, R. Louis. Prognostic factors in non small cell lung cancer. *Rev méd Liège*. 71:34–9 (2016)

36. SR. Kang, HC. Song, BH. Byun, JR. Oh, HS. Kim, SP. Hong, SY. Kwon, A. Chong, J. Kim, SG. Cho *et al.* Intratumoral Metabolic Heterogeneity for Prediction of Disease Progression After Concurrent Chemoradiotherapy in Patients with Inoperable Stage III Non-Small-Cell Lung Cancer. *Nucl Med Mol Imaging*.48:16–25 (2014)

37. T. Win, KA. Miles, SM. Janes, B. Ganeshan, M. Shastry, R. Endozo, M. Meagher, RI. Shortman, S. Wan, I. Kayani *et al.* Tumor heterogeneity and permeability as measured on the CT component of PET/CT predict survival in patients with non-small cell lung cancer. *Clin Cancer Res*. 19:3591–9 (2013)

38. M. Vaidya, KM. Creach, J. Frye, F. Dehdasht, JD. Bradley, I. El Naqa. Combined PET/CT image characteristics for radiotherapy tumor response in lung cancer. *Radiother Oncol*. 102:239–45 (2012)

39. GJ. Cook GJ, ME. O'Brien, M. Siddique, S. Chicklore, HY. Loi, B. Sharma, R. Punwani, P. Bassett, V. Goh, S. Chua. Non – Small Cell Lung Cancer Treated with Erlotinib: Heterogeneity of 18 F-FDG Uptake at Response and Prognosis 1. *Radiology*. 276:883–93 (2015)

40. N. Ohri, F. Duan, BS. Snyder, B. Wei, M. Machtay, A. Alavi, BA. Siegel, DW. Johnson, JD. Bradley, A. DeNittis *et al.* Pretreatment 18FDG-PET Textural Features in Locally Advanced Non-Small Cell Lung Cancer: Secondary Analysis of ACRIN 6668/RTOG 0235. *J Nucl Med*. 57:842–8 (2016)

41. DH. Kim, J. Jung, SH. Son, CY. Kim, CM. Hong, JR. Oh, SY. Jeong, SW. Lee, J. Lee, BC. Ahn. Prognostic Significance of Intratumoral Metabolic Heterogeneity on 18F-FDG PET/CT in Pathological N0 Non–Small Cell Lung Cancer. *Clin Nucl Med*. 40:708–14 (2015)

42. RM Kessler, JR. Ellis, M. Eden. Analysis of emission tomographic scan data: limitations imposed by resolution and background. *J Comput Assist Tomogr*. 8:514–22 (1984)

43. FH. van Velden, P. Cheebsumon, M. Yaqub, EF. Smit, OS. Hoekstra, AA. Lammertsma, R. Boellaard. Evaluation of a cumulative SUV-volume histogram method for parameterizing heterogeneous intratumoural FDG uptake in non-small cell lung cancer PET studies. *Eur J Nucl Med Mol Imaging*. 38(9):1636–47 (2011)

44. M. Hatt, M. Majdoub, M. Vallières, F. Tixier, CC. Le Rest, D. Groheux, E. Hindié, A. Martineau, O. Pradier, R. Hustinx *et al.* 18F-FDG PET uptake characterization through texture analysis: investigating the complementary nature of heterogeneity and functional tumor volume in a multi-cancer site patient cohort. *J Nucl Med*. 56:38–44 (2015)

45. S. Yip, K McCall, M Aristophanous, AB Chen, HJ Aerts, R Berbeco. Comparison of texture features derived from static and respiratory-gated PET images in non-small cell lung cancer. *PLoS One*. 9(12):e115510 (2014)

46. NM. Cheng, YH. Fang, DL. Tsan, CH. Hsu, TC. Yen. Respiration-Averaged CT for Attenuation Correction of PET Images - Impact on PET Texture Features in Non-Small Cell Lung Cancer Patients. *PLoS One*. 11(3):e0150509 (2016)

47. W. Grootjans W, F. Tixier, CS. van der Vos, D. Vriens, CC. Le Rest, J. Bussink, WJ. Oyen, LF. de Geus-Oei, D. Visvikis, EP. Visser. The Impact of Optimal Respiratory Gating and Image Noise on Evaluation of Intratumor Heterogeneity on 18F-FDG PET Imaging of Lung Cancer. *J Nucl Med*. 57(11):1692–1698 (2016)

48. M. Carles, I. Torres-Espallardo, U. Nestle, L. Martí-Bonmatí. Optimizing 4D-PET/CT Imaging for Heterogeneity Quantification by Texture Features. *IEEE* Nuclear Science Symposium and Medical Imaging Conference Record (NSS/MIC), M04E-13–24 (2016)

49. I. Buvat, F. Orlhac, M. Soussan. Tumor Texture Analysis in PET: Where Do We Stand? *J Nucl Med*. 56:1642–4 (2015)

Key Words: Lung cancer, Non small cell lung cancer, PET/CT, Texture, Radiomics, Diagnosis

Send correspondent to: Margarita Kirienko, Department of Biomedical Sciences, Humanitas University, Rozzano, Milan, Italy, Tel: 390282246621, Fax: 390282246693, E-mail: margarita.kirienko@icloud.com